Monorail vehicle model to study influence of tyre modelling on overall dynamics

Gabriel P.R. Maciel* and
Roberto Spinola Barbosa

Polytechnic School of the University of São Paulo,
Av. Prof. Mello Moraes, 2231, Sao Paulo, SP,
cep.: 05508-970, Brazil
Email: ga.pe.01@gmail.com
Email: spinola@usp.br
*Corresponding author

Abstract: A mathematical model of a straddle type monorail vehicle has been developed in order to study its stability and the effect of tyre modelling techniques on its dynamic response. An algorithm was developed to build equations of motion using a multi-body systems method, considering deviations of the guideway as forced inputs. Tyre models consider both radial and lateral forces. Four methods to calculate lateral forces were implemented and results were compared. One of the four vehicle models is linear and parameterised with the longitudinal velocity, enabling the stability analysis based on eigenvalues locus. The modal damping decreases with the increase of longitudinal velocity, asymptotically approaching to a stable system. Results show that the influence of tyre radial force on its cornering stiffness can be an important effect to consider in the monorail numerical modelling, increasing the accuracy to predict the vehicle overall dynamics and tyre lateral forces.

Keywords: dynamic; vehicle; monorail; tyre; modelling.

Reference to this paper should be made as follows: Maciel, G.P.R. and Barbosa, R.S. (2016) 'Monorail vehicle model to study influence of tyre modelling on overall dynamics', *Int. J. Heavy Vehicle Systems*, Vol. 23, No. 4, pp.317–332.

Biographical notes: G.P.R. Maciel is postgraduate student in the Group of Dynamic and Control of the Mechanical Engineering Department of the Polytechnic School of São Paulo University, Brazil. His research interests are on dynamics of multibody systems, vibration, vehicle dynamics and structural analysis.

R.S. Barbosa is a Professor in the Group of Dynamic and Control of the Mechanical Engineering Department of the Polytechnic School of São Paulo University, Brazil. He worked for 20 years on the Research Institute of Technology of Sao Paulo, dealing with vibration, comfort and safety on railway vehicles in the Transport Division. He received his PhD from the University of Sao Paulo and DSc from the University of Campinas in Sao Paulo, Brazil. His research interests are on dynamics of multibody systems, vibration and vehicle dynamics.

1 Introduction

With the growth of big cities, the demand to increase the capacity of transport systems has been pushing engineers to develop faster, larger, safer and more comfortable vehicles. In this context, multi-body vehicle dynamics simulation has a major importance in vehicle design, helping the validation of vehicle performance before a prototype is built. Multi-body simulation allows prediction of vehicle stability and safety limits, evaluation of ride quality, determination of design loads for component durability analysis, etc. It is reasonable that the above-mentioned applications require a high degree of trustworthiness and similarity when compared to a real vehicle, since significant deviation of simulation results from real vehicle behaviour may lead to troubleshooting in the late stages of design. Considering this, determination of accurate techniques for building a virtual model is one main challenge in vehicle virtual modelling and simulation.

A review about different techniques for modelling suspension components and the impact of more detailed models in the overall vehicle dynamics was presented by Bruni et al. (2011). Literature indicating that contact forces play an important role in vehicle dynamics is abundant (Cao et al., 2011; Mohajer et al., 2015) while discussions about adequate level of detail for modelling contact forces and its impact on the overall simulation accuracy is limited for applications on straddle type monorail vehicles.

The level of detail of contact forces modelling on road and rail vehicles stability is discussed by Shen et al. (2007) and Polach (2007) respectively.

The necessity of the accurate calculation of tyre forces is discussed by Du et al. (2014), which shows methods to calculate tyre wear on monorail vehicles and how it is influenced by changes in suspension parameters.

In a recent work (Wei and Dorfi, 2014), the influence of tyre transient lateral force on road vehicle dynamics was studied and it was showed that it has a relatively small contribution to vehicle handling performance compared with the tyre steady-state force. This type of study provides important guidelines for the best practices of numerical modelling techniques.

Liu et al. (2014) studied the effect of wheel pressure on vibration of straddle type monorail vehicles. In this paper, it was showed that the influence of vertical, guide and stabilising tyre pressures has a considerable influence on the response of the system, such as at tyre radial forces and car body displacements.

This work intends to review modelling techniques to predict the dynamic behaviour and stability of monorail vehicles and discuss the level of detail of tyre models considering the expected overall accuracy of the virtual vehicle.

There are two types of vehicles used in monorail systems: hanging type and straddle type. The hanging type has its centre of mass under the guideway and runs hanged under it. The straddle type has the vehicle's centre of mass above the guideway and runs on it. The guideway is built using beams that are aligned to each other in order to form a long path of several beams. These beams can be misaligned due to different causes: assembling precision, different radius concordance, curve transitions, thermal expansion, etc. These misalignments will be further simulated in this work in order to evaluate and compare vehicle's transient response.

In this paper, a virtual straddle type monorail vehicle was modelled using different tyre modelling techniques in order to verify the influence of these different approaches on the representation of vehicle dynamics. It is expected that an investment in modelling more detailed components shall add more accuracy to simulation results and vehicle's behaviour. This statement will be used to evaluate the application of modelling techniques due to its

impact on results when compared to less detailed models. Equations of motion were built using multi-body systems (MBS) method, considering deviations of the guideway as forced inputs. Figure 1 shows an example of a straddle type monorail vehicle.

Figure 1 Straddle-type monorail vehicle

2 System description

Figure 2 shows the front view of the model used for dynamic simulation of a monorail vehicle. The model represents half vehicle and is composed by one car body which is assumed to be a rigid body with three degrees of freedom: lateral displacement (y), vertical displacement (z) and roll angle (θ). It is considered that the car body moves forward with a constant velocity V_x.

There are two main Cartesian coordinate systems in the model: one is attached to the car body (Goda et al., 2000; Shabana, 2008) (with centre at point O_c, positioned at car's centre of mass) and another moves along the line at the middle of upper surface of the guideway at the same longitudinal velocity as the car body (with centre at point O_g).

The car body interacts with the guideway trough vertical tyres and horizontal tyres shown in Figure 2. Vertical tyres support the vertical load of the vehicle (indicated by letter p). Guide tyres and stabilising tyres, guide the car body along the guideway (indicated by letters q and r, respectively). The main function of stabilising tyres is to prevent excessive rolling of the car body (Goda et al., 2000). It was considered that each tyre has one point of contact with the guideway surface, defined as ij where i is the corresponding tyre pair letter and j is the tyre number $j = 1, 2$. Each tyre interacts with the guideway with two contact forces: radial and lateral, indicated in Figure 2 as F_{rij} and F_{sij} respectively. All properties and forces are indicated with letters i and j which correspond to the tyre position.

In the virtual model, generalised coordinates are: y for lateral displacement, z for vertical displacement and θ for roll rotation of the car body. Forced inputs x_r are herein representing guideway deviations to a perfectly straight path and are considered small when compared to other displacements.

$$x(t) = \{\, y(t)\; z(t)\; \theta(t) \,\}^T \qquad x_r(t) = \{\, y_r(t)\; z_r(t)\; \theta_r(t) \,\}^T.$$

Figure 2 Dynamic model of monorail car

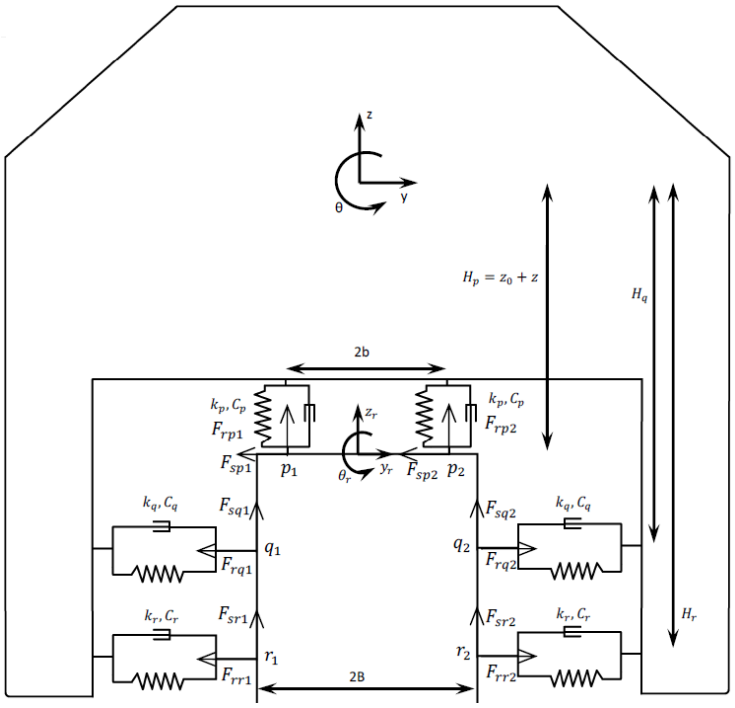

2.1 Tyre forces

Two types of forces are calculated for each tyre: radial and lateral. Radial force is a force reaction of the tyre against the guideway surface in radial direction to the respective tyre acting on the tyre contact point. Lateral forces are generated by lateral slippage in the contact point between tyre and guideway.

2.1.1 Radial forces

The same radial force method was used in all four models in this work. A virtual body is attached to the point of contact of each tyre tread with the guideway. These virtual bodies move along the surface of the guideway and have no mass. A virtual body is connected to the car body through a spring and damper, which causes internal forces at the system when there are relative displacements and/or velocities between virtual bodies and car body.

$$F_{rij} = F^0_{rij} + k_i \Delta S_{rij} + c_i \frac{\partial \Delta S_{rij}}{\partial t}, \tag{1}$$

where F^0_{rij} is the radial preload force and ΔS_{rij} is the relative displacement between virtual body and car body.

2.1.2 Lateral forces

In order to calculate tyre slippage, necessary to calculate lateral forces, a local coordinate system called ‘tyre frame’ was attached at each virtual body and has the same orientation

of guideway coordinate system. Lateral forces due to slip act on virtual bodies when there is a slippage between the corresponding tyre and guideway. It is assumed that longitudinal velocity of car body is constant and tyres roll with constant angular velocity so that there is no longitudinal slippage. Although movements of car body with respect to the guideway can produce lateral slippage at tyres. The direction of lateral slip velocities is parallel to slip forces with opposite orientation.

Figure 3 shows a schematic top view of a tyre (represented with thick lines) with slip forces and velocities oriented in tyre reference frame, where V is the total velocity of contact point, V_{sij} is the lateral slip velocity of tyre ij and lateral slip angle α is the ratio of lateral and longitudinal velocity of tyre. Tyre lateral force is proportional to lateral slip α and cornering stiffness as described in equation (2) (Pacejka, 2005).

$$F_{sij} = \alpha k_{sij}. \tag{2}$$

Later in this work, different methods will be presented as a variation of computing lateral slip velocities and cornering stiffness.

Figure 3 Slip velocities and forces at tyre

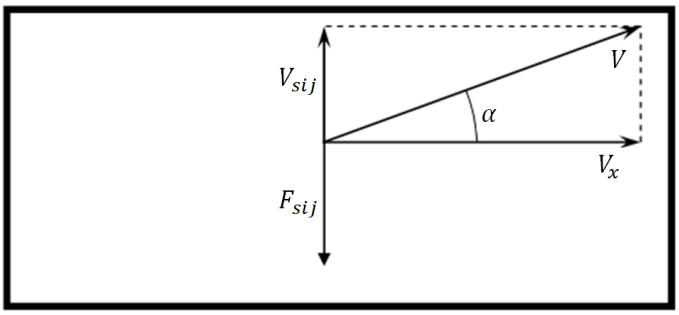

2.2 Equations of motion

Equations of motion are written as function of mass matrix $[M]$, damping matrix $[C]$, stiffness matrix $[K]$ and generalised external forces Q_{ext}, which is composed by tyre lateral slip forces.

$$[M]\ddot{x} + [C]\dot{x} + [K]\,(x - x_r) = Q_{\text{ext}}, \tag{3}$$

where

$$\begin{bmatrix} M & 0 & 0 \\ 0 & M & 0 \\ 0 & 0 & I_x \end{bmatrix} \begin{bmatrix} \ddot{y} \\ \ddot{z} \\ \ddot{\theta} \end{bmatrix} + \begin{bmatrix} 2(c_q + c_r) & 0 & 2(H_q c_q + H_r c_r) \\ 0 & 2c_p & 0 \\ 2(H_q c_q + H_r c_r) & 0 & 2(H_q^2 c_q + H_r^2 c_r + b^2 c_p) \end{bmatrix} \begin{bmatrix} \dot{y} \\ \dot{z} \\ \dot{\theta} \end{bmatrix} +$$

$$\begin{bmatrix} 2(k_q + k_r) & 0 & 2(H_q k_q + H_r k_r) \\ 0 & 2k_p & 0 \\ 2(H_q k_q + H_r k_r) & 0 & 2(H_q^2 k_q + H_r^2 k_r + b^2 k_p) \end{bmatrix} \left(\begin{bmatrix} y \\ z \\ \theta \end{bmatrix} - \begin{bmatrix} y_r \\ z_r \\ \theta_r \end{bmatrix} \right) = \begin{bmatrix} Q_y \\ Q_z \\ Q_\theta \end{bmatrix}.$$

In order to simulate the system of equations in the time domain, equation (3) was rearranged into a first order dynamical system on the state space (Barbosa and Neto, 1996) domain as follows:

$$\dot{X} = \begin{bmatrix} -[M]^{-1}[C] & -[M]^{-1}[K] \\ [I] & [0] \end{bmatrix} X + \begin{bmatrix} [M]^{-1}[K] \\ 0 \end{bmatrix} x_r + \begin{bmatrix} [M]^{-1} \\ 0 \end{bmatrix} Q_{\text{ext}}, \tag{4}$$

where $[I]$ is identity matrix and $X(t) = \{\dot{y}(t), \dot{z}(t), \dot{\theta}(t), y(t), z(t), \theta(t)\}^T$ is the vector that defines the state of the dynamical system at a specified time t.

3 Linearised model (Model 1)

In order to study the influence of tyre modelling on monorail vehicle dynamics, different complexity models were used. System performance was evaluated from a linear model to a complete high order non-linear model.

The first model described is completely linear, with the advantage to perform a stability analysis based on eigenvalues locus in complex plane.

3.1 Cornering stiffness – linear method

In model 1, cornering stiffness k_{sij} was modelled as a constant value.

3.2 Slip velocities – linear method

Taking as an example V_{sp1}, the lateral slip velocity of point P1, aligned to axis Z_r, it's possible to observe that this relation is nonlinearly dependent to the generalised coordinates.

$$V_{sp1} = \dot{y} - \dot{\theta}\left(z_0 + z + \frac{b^2}{z_0 + z}\right). \tag{5}$$

In the linear approach, it was considered that the magnitudes of generalised coordinates at the system are sufficiently small that second order terms were neglected. Using this statement, equation (5) can be linearised leading to linearly dependent slip velocities in respect to generalised coordinates.

$$V_{sp1} = \dot{y} - \dot{\theta}\left(z_0 + \frac{b^2}{z_0}\right). \tag{6}$$

The same approach of equation (6) can be done for all contact points, resulting in a set of linear dependent equations to calculate slip velocities and the resulting relations are called in this work as linear method to calculate slip velocities.

3.3 State space representation

Second order terms are also neglected in order to calculate generalised forces, which are linearly dependent to generalised coordinates.

$$\begin{bmatrix} Q_y \\ Q_z \\ Q_\theta \end{bmatrix} = \begin{bmatrix} F_{sp1} + F_{sp2} \\ F_{sq1} + F_{sq2} + F_{sr1} + F_{sr2} \\ z_0 F_{sp1} + z_0 F_{sp2} - BF_{sq1} + BF_{sq2} - BF_{sr1} + BF_{sr2} \end{bmatrix}. \tag{7}$$

Substituting equation (7) in equation (3), we have:

$$[M]\ddot{x} + \left([C] + \frac{1}{|V_x|}[C_{nc}]\right)\dot{x} + [K](x - x_r) = 0. \tag{8}$$

With

$$[C_{nc}] = \begin{bmatrix} -2k_{sp} & 0 & 2k_{sp}\left(z_0 + \frac{b^2}{z_0}\right) \\ 0 & -2(k_{sq} + k_{sr}) & 0 \\ -2k_{sp}z_0 & 0 & 2k_{sp}(z_0^2 + b^2) - 2k_{sq}(B^2 + H_q^2) - 2k_{sr}(B^2 + H_r^2) \end{bmatrix}.$$

Writing equation (8) in the form of equation (4), it's possible to see that we have a linear dynamic system with the following state space structure:

$$\dot{X} = \begin{bmatrix} -[M]^{-1}[\bar{C}] & -[M]^{-1}[K] \\ [I] & [0] \end{bmatrix} X + \begin{bmatrix} [M]^{-1}[K] \\ 0 \end{bmatrix} x_r, \tag{9}$$

where $[\bar{C}] = [C] + |V_x|^{-1}[C_{nc}]$, $X = \{\dot{x} \quad x\}^T$ and $u = \{x_r \quad 0\}^T$.

4 Complete models

4.1 Cornering stiffness – complete method

The cornering stiffness linear method assumes that cornering stiffness is constant, although linearised modelling can be sufficient in the neighbourhood of design configuration but can have discrepancies if nonlinearities are significant. Moreover it is known that lateral forces are influenced by tyre radial forces (Segel and Ervin, 1981). Using these assumptions, the complete method assumes that the cornering stiffness is influenced by changes in the radial tyre force as described in equation (10) (Pacejka, 2005), where c_{1i} and c_{2i} are constants for each tyre:

$$k_{sij}(F_{rij}) = c_{1i} \sin\left(2 \arctan\left(\frac{F_{rij}}{c_{2i}}\right)\right). \tag{10}$$

4.2 Slip velocities – complete method

The complete method to calculate slip velocities considers that the magnitude of generalised coordinates is not small enough to neglect higher order terms, so slip velocities will be calculated as in equation (5). As a consequence, generalised external forces and moments are calculated as in equation (12) in order to keep consistency with the consideration of higher order terms.

$$\begin{aligned} Q_y &= F_{sp1} + F_{sp2} \\ Q_z &= F_{sq1} + F_{sq2} + F_{sr1} + F_{sr2} \\ Q_\theta &= (z_0 + z)F_{sp1} + (z_0 + z)F_{sp2} - (B + y)F_{sq1} \\ &\quad + (B - y)F_{sq2} - (B + y)F_{sr1} + (B - y)F_{sr2}. \end{aligned} \tag{11}$$

4.3 Preload forces

Tyre cornering stiffness is influenced by radial force and consequently by the radial preload force. The determination of vertical tyres radial preload force can be done based on vehicle's weight, although guiding and stabilising tyres radial preload forces have to be determined as a design parameter that influences vehicles' dynamic response.

Based on equation (10), the maximum value of cornering stiffness is equal to the coefficient c_1. If the cornering stiffness reaches its maximum value, it decreases if the radial force increases. It means that the tyre starts to loose its capacity to generate lateral forces, which is not a desirable behaviour.

Figure 4 shows the variation of the cornering stiffness (normalised by the coefficient c_1) according to radial force (normalised by the coefficient c_2). This relation was calculated using equation (10).

Figure 4 Normalised cornering stiffness in respect to normalised radial force

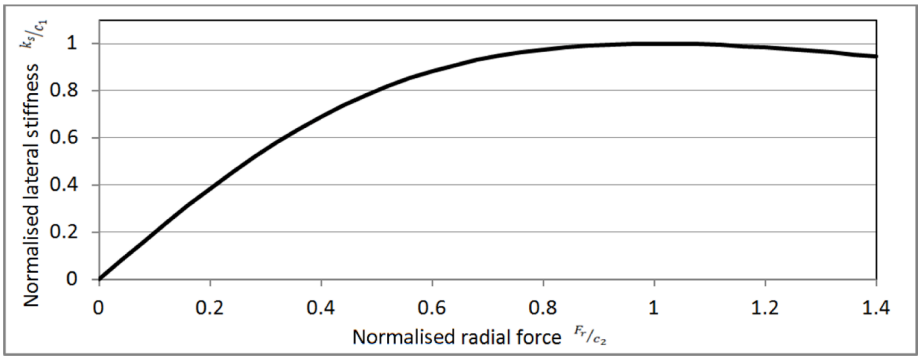

Considering this, the tyre radial force preload has to be specified in a way to produce an initial cornering stiffness not too small but not too close to the maximum value. The authors propose a method to determine the preload radial force by imposing an initial value of cornering stiffness.

Given an arbitrary value of the normalised cornering stiffness, equation (10) can be written as a function of this value. As a contribution to this work, the authors propose a normalised cornering stiffness equals to $\frac{3}{4}c_1$. This means that the preload radial force corresponds to an initial cornering stiffness equal to $\frac{3}{4}$ of the maximum saturation value.

$$F_{rij}^{0} = c_{2i} \tan\left[\tfrac{1}{2} \arcsin\left(\tfrac{3}{4}\right)\right]. \tag{12}$$

4.4 Dynamic models

Four different methodology combinations were evaluated in order to study the effects of tyre modelling techniques. Each one has a different methodology to calculate slip forces at tyres. Table 1 shows the combinations of cornering stiffness and slip velocities methods.

Table 1 Numerical models and corresponding modelling techniques

Model number	*Cornering stiffness*	*Slip velocities*
Model 1	Linear	Linear
Model 2	Linear	Complete
Model 3	Complete	Linear
Model 4	Complete	Complete

5 Results

5.1 Modal analysis and stability

From the linear system (Model 1) described in equation (9), three pairs of complex conjugate eigenvectors can be found, describing three eigenmodes. One eigenmode called lower sway vehicle body movement, determined by the eigenvector, is characterised by phase movement of lateral displacement (y coordinate) and the body angular rolling (θ coordinate) while the vertical displacement (z coordinate) remains in a smaller amplitude (Figure 5 (left)). The eigenmode upper sway is characterised by the opposite phase of y and θ at the eigenvector while z remains in a smaller amplitude (Figure 5 (centre)). At bounce eigenmode, the amplitude of z in the eigenvector is dominant and y and θ are almost imperceptible (Figure 5 (right)).

Figure 5 Eigenmodes of vehicle. (left) lower sway, (centre) upper sway and (right) bounce

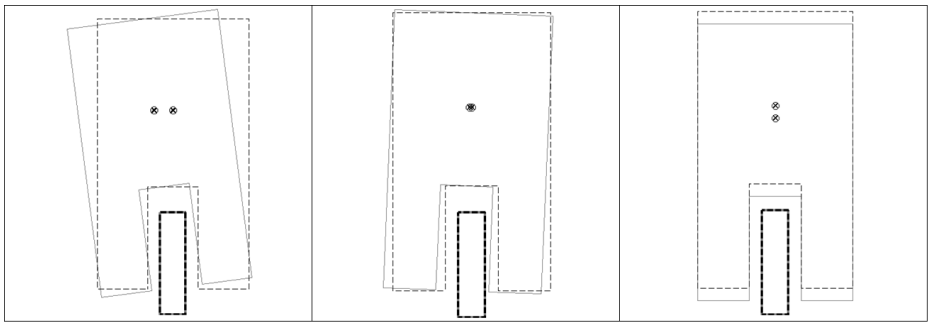

It is possible to verify from the equation (8) that there's a term that depends on the longitudinal velocity of the car body, so the eigenvalues of the system will be influenced by this parameter. Figure 6 shows the location of the system's poles due to a variation of longitudinal velocity V_x from 4 m/s to 30 m/s. Arrows in this figure indicates the path that poles make while longitudinal velocity is increased.

It's also possible to see that in equation (8), the term $1/|V_x|\ [C_{nc}]$ decreases with the increment of the longitudinal velocity, asymptotically approaching to zero. With this statement, it's possible to conclude that $[\bar{C}] \cong [C]$ and the poles of the system at Figure 6

asymptotically approach to the poles of the system described at equation (13) with the increment of longitudinal velocity.

$$\dot{X} = \begin{bmatrix} -[M]^{-1}[C] & -[M]^{-1}[K] \\ [I] & [0] \end{bmatrix} X + \begin{bmatrix} [M]^{-1}[K] \\ 0 \end{bmatrix} x_r. \tag{13}$$

Observing the real part of the eigenvalues in Figure 6, it is possible to conclude that the system is stable in the whole investigated range of speeds up to 108 km/h. Considering that the system in equation (13) is stable, it's also possible to conclude that increasing longitudinal velocity, the monorail vehicle will be stable as well. Figure 7 shows the values of natural frequencies and damping factors of the eigenmodes with the longitudinal velocity increase.

Figure 6 Location of system's poles due to increment of longitudinal velocity (x marks)

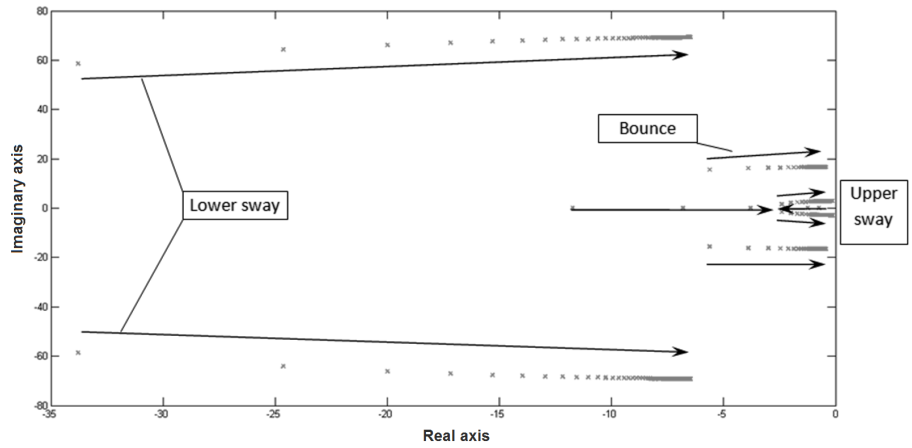

5.2 *Time transient simulations*

In order to evaluate and compare the transient response of the models, two types of forced inputs at the system are proposed. The first input emulates a misalignment between two consecutive beams along the guideway. The first forced input is a lateral misalignment beam transition of 10 mm, which can be modelled as a lateral step input at vector x_r as follows.

$$\begin{cases} x_r(t < 0.1) = \{0 \quad 0 \quad 0\}^T \\ x_r(t \geq 0.1) = \{10 \quad 0 \quad 0\}^T. \end{cases}$$

From Figure 8, it's possible to see that in models 3 and 4, a disturbance in lateral direction leads to a significant displacement in z direction. This behaviour is caused by the variation of the tyre cornering stiffness due to changes in its radial force. When the vehicle is subjected to a lateral step disturbance, tyre forces cause a momentum at car body leading it to start a roll rotation. The roll velocity leads to slippage at guide and stabilising tyres, which are deflected differently by the lateral disturbance. With different radial forces at left and right tyres, different slip forces will be generated at the vertical direction, leading to vertical acceleration (and consequently vertical displacement) of car body.

Figure 7 Natural frequencies and damping factors due to increment of longitudinal velocity

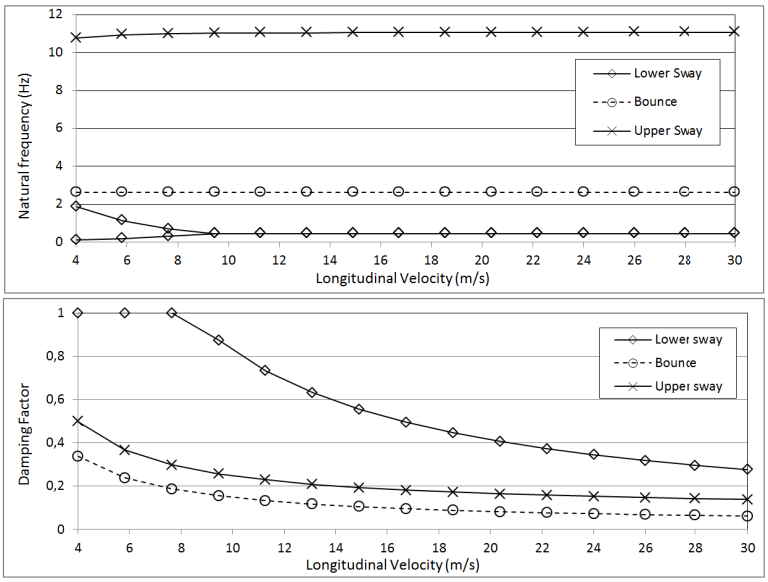

Figure 8 Lateral (top) and vertical (centre) displacements and roll rotation (bottom) – lateral step input (see online version for colours)

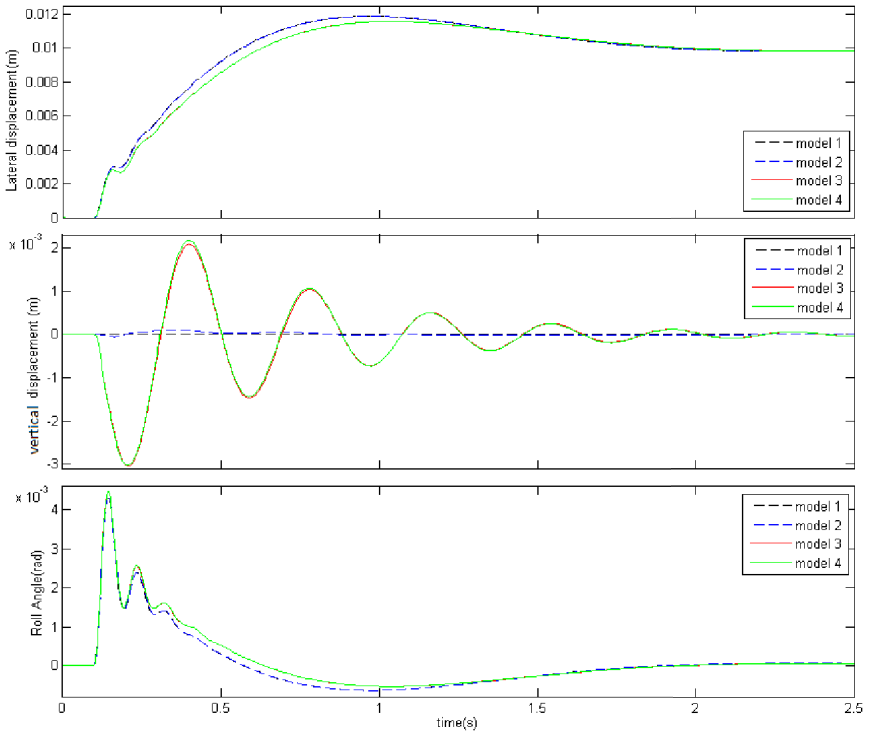

The aforementioned behaviour characterises a nonlinear coupling between lateral and vertical movements of the car body, which is reproduced if the complete cornering stiffness model, described in item 4.1, is adopted. For models where constant cornering stiffness is adopted, this behaviour is non-existent for model 1 and small for model 2.

In order to determine a numerical comparison between models, a parameter e_d was proposed to quantify the relative deviation of the model 4 (with complete methods for cornering stiffness and slip velocities) to the models 1, 2 and 3. Radial and lateral forces at tyres were measured and the maximum value was normalised in respect to the equivalent maximum force at model 4. As stated below for $k = 1, 2, 3$.

$$e_d = \frac{F_k^{\max} - F_4^{\max}}{F_4^{\max}}$$

Figure 9 shows the comparison of lateral force F_{sq1}, which does not increase in models 3 and 4 as fast as it does in models 1 and 2. This effect is caused by the variation of cornering stiffness considered in models 3 and 4 but not considered in models 1 and 2. During transient response, tyre Q_1 radial force decreases, decreasing cornering stiffness and reducing its ability to generate lateral forces.

Figure 9 Lateral force F_{sq1} – lateral step input (see online version for colours)

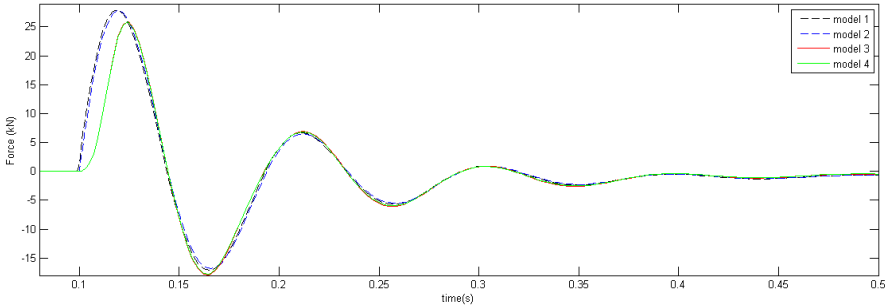

Figure 10 shows the cornering stiffness k_{sq1} value during the lateral step input simulation. The values corresponding to models 1 and 2 are constant as expected. Although in models 3 and 4, there is a variation of approximately 97% and 18% (in respect of the initial value) in $t = 0.1$ s and $t = 0.19$ s respectively.

Figure 10 Cornering stiffness k_{sq1} – lateral step input (see online version for colours)

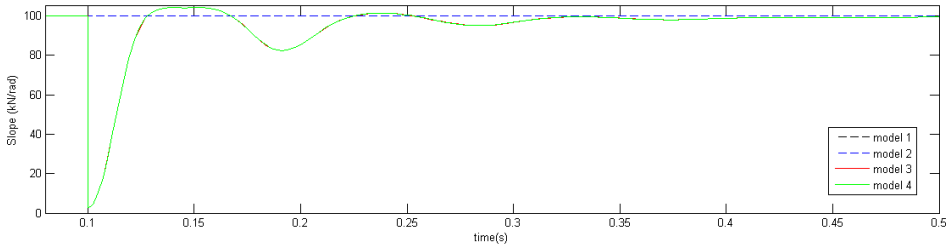

Analysing Table 2, one can observe that the maximum deviation of the radial force predicted with the linear model is –6.8% and the maximum deviation of the slip force is 8.1%.

Table 2 Percentage deviation from the complete model 4 – maximum radial force and maximum absolute lateral force – lateral step

	Unit	*Model 1* (%)	*Model 2* (%)	*Model 3* (%)
Max radial force F_{rp1}	kN	–6.7	–6.7	0.0
Max radial force F_{rp2}	kN	–6.8	–6.8	0.0
Max radial force F_{rq1}	kN	–1.6	–1.6	0.0
Max radial force F_{rq2}	kN	0.0	0.0	0.0
Max radial force F_{rr1}	kN	–1.4	–1.4	0.0
Max radial force F_{rr2}	kN	0.0	0.0	0.0
Max abs lateral force F_{sp1}	kN	–6.6	–6.6	0.0
Max abs lateral force F_{sp2}	kN	–6.1	–6.1	0.0
Max abs lateral force F_{sq1}	kN	8.1	8.1	0.4
Max abs lateral force F_{sq2}	kN	–7.6	–7.3	–0.3
Max abs lateral force F_{sr1}	kN	0.4	0.0	0.4
Max abs lateral force F_{sr2}	kN	–7.7	–7.5	–0.2

The second forced input is a lateral and vertical misalignment beam transition of 10 mm in both lateral and vertical directions, which can be modelled as a lateral step input at vector x_r as follows.

$$\begin{cases} x_r(t < 0.1) = \{0 \quad 0 \quad 0\}^T \\ x_r(t \geq 0.1) = \{10 \quad 10 \quad 0\}^T. \end{cases}$$

Figure 11 shows lateral and vertical displacements and roll rotation angle for the combined vertical and lateral step input. Figure 12 shows the comparison of lateral force F_{sq2}, the maximum values are higher in models 3 and 4.

Analysing Table 3, one can observe that the maximum deviation of the radial force predicted with the linear model is –2.9% and the maximum deviation of the slip force is –10.1%.

Table 3 Percentage deviation from the complete model 4 – maximum radial force and maximum absolute lateral force – combined lateral and vertical step

	Unit	*Model 1* (%)	*Model 2* (%)	*Model 3* (%)
Max radial force F_{rp1}	kN	2.3	2.5	–0.1
Max radial force F_{rp2}	kN	1.6	2.1	–0.6
Max radial force F_{rq1}	kN	–2.9	–2.9	0.0
Max radial force F_{rq2}	kN	–1.2	–1.2	0.0
Max radial force F_{rr1}	kN	0.0	0.0	0.0
Max radial force F_{rr2}	kN	–1.5	–1.5	0.0
Max abs lateral force F_{sp1}	kN	0.0	0.0	0.0
Max abs lateral force F_{sp2}	kN	–1.9	–1.9	0.0
Max abs lateral force F_{sq1}	kN	0.0	0.0	0.0
Max abs lateral force F_{sq2}	kN	–10.1	–10.1	0.0
Max abs lateral force F_{sr1}	kN	–10.1	–10.1	0.0
Max abs lateral force F_{sr2}	kN	7.8	7.5	0.4

Figure 11 Lateral (top) and vertical (centre) displacements and roll rotation (bottom) – lateral and vertical step input (see online version for colours)

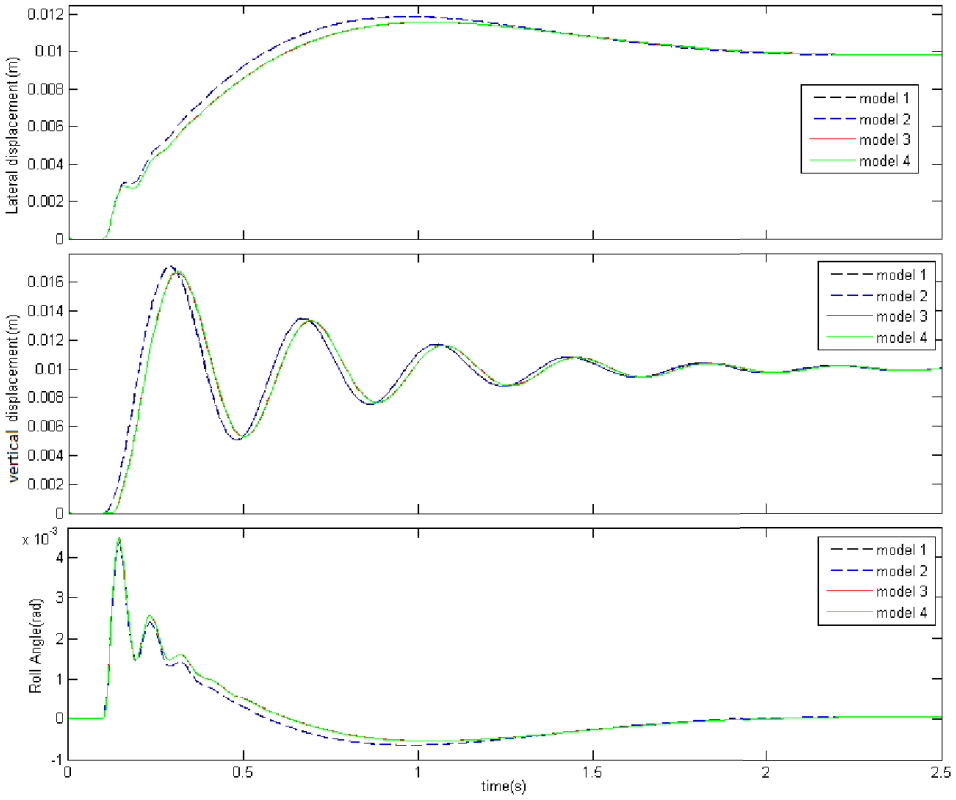

Figure 12 Lateral force F_{sq2} – combined lateral and vertical step input (see online version for colours)

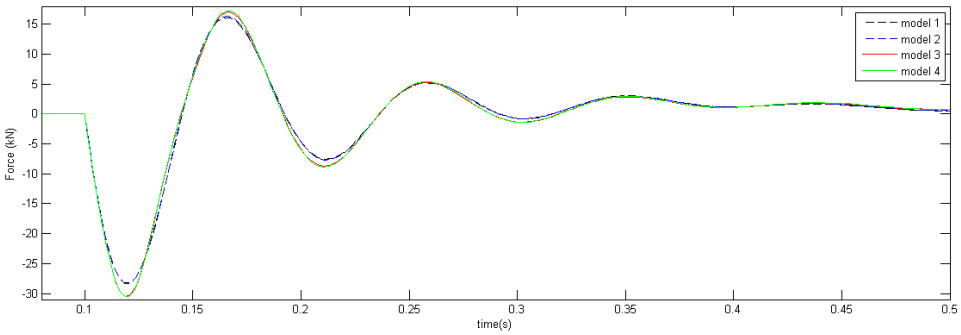

Table 4 shows the properties used in the simulated monorail vehicle models.

Table 4 Model parameters

Parameter name	*Variable*	*Unit*	*Value*
Car body mass (half vehicle)	M	kg	9450
Car body roll inertia (half vehicle)	I_x	kg.m^2	10,000
Stiffness of vertical tyre in radial direction	k_p	N/m	$1.3\dot{1}0^6$
Stiffness of guide tyre in radial direction	k_q	N/m	$1.3\dot{1}0^6$
Stiffness of stabilising tyre in radial direction	k_r	N/m	$1.3\dot{1}0^6$
Damping coefficient of vertical tyre in radial direction	c_p	N.s/m	3180
Damping coefficient of guide tyre in radial direction	c_q	N.s/m	3180
Damping coefficient of stabilising tyre in radial direction	c_r	N.s/m	3180
Tyre cornering stiffness (vertical, guide and stabilising)	$k_{s(p,q,r)}$	N/rad	10^5
Vertical distance of car body centre of mass and guide tyre	H_q	m	2.5
Vertical distance of car body centre of mass and stabilising tyre	H_r	m	3.2
Half of guideway width	B	m	0.25
Half of distance between vertical tyres	b	m	0.185
Initial vertical position of car body centre of mass	z_0	m	2.0
Vertical tyre radial preload force	$F^0_{rp(1,2)}$	N	46,352
Guide tyre radial preload force	$F^0_{rq(1,2)}$	N	13,244
Stabilising tyre radial preload force	$F^0_{rr(1,2)}$	N	13,244
Vertical tyre cornering stiffness coefficient 1	c_{1p}	–	$1.04\dot{1}0^5$
Vertical tyre cornering stiffness coefficient 2	c_{2p}	–	61,803
Guide tyre cornering stiffness coefficient 1	c_{1q}	–	$1.04\dot{1}0^5$
Guide tyre cornering stiffness coefficient 2	c_{2q}	–	17,658
Stabilising tyre cornering stiffness coefficient 1	c_{1r}	–	$1.04\dot{1}0^5$
Stabilising tyre cornering stiffness coefficient 2	c_{2r}	–	17,658

6 Conclusions

A model of a straddle type monorail vehicle was developed with three degrees of freedom representing a frontal half vehicle. As a contribution to this work, the authors introduced a method to determine the guiding and stabilising tyres radial preload forces, based on the tyre properties.

The linear modal behaviour of the vehicle was analysed and the stability based on root locus reveals that the vehicle's pole placement is considerably influenced by its longitudinal velocity. It was showed that lower sway and upper sway vibration modes' natural frequencies and damping factors decrease with the increase of longitudinal velocity, asymptotically approaching to a stable system.

Results show that the tyre modelling technique influences the overall dynamics of a straddle type monorail vehicle numerical model. The influence of tyre radial force on its cornering stiffness has a great effect on the vehicle's overall dynamics. It induces a nonlinear coupling between lateral and vertical movements of the car body, when the vehicle passes through a lateral misalignment at the guideway.

In the simulation of lateral misalignment between two consecutive beams, the maximum deviations of radial and slip forces were –6.8% and 8.1% respectively. In the simulation of

lateral and vertical misalignment beam transition, maximum deviations of radial and slip forces were –2.9% and –10.1% respectively. These differences can be important to develop a virtual model that predicts the real vehicle's behaviour with more accuracy. Moreover, increasing the accuracy to predict tyre lateral and vertical forces can be useful specially to predict tyre durability.

It's also important to notice that the maximum forces are very similar between models 3 and 4 for both simulations. So in the circumstances to which the vehicle was subjected, the implementation of the complete slip velocities contributes very little to the numerical response accuracy of the model.

References

Barbosa, R.S. and Neto, A.C. (1996) 'Dinâmica do rodeiro ferroviário', *Revista Brasileira de Ciências Mecânicas*, Vol. 18, No. 4, pp.318–329.

Bruni, S., Vinolas, J., Berg, M., Polach, O. and Stichel, S. (2011) 'Modelling of suspension components in a rail vehicle dynamics context', *Vehicle System Dynamics: International Journal of Vehicle Mechanics and Mobility*, Vol. 49, No. 7, pp.1021–1072.

Cao, D., Song, X. and Ahmadian, M. (2011) 'Editors' perspectives: road vehicle suspension design, dynamics, and control', *Vehicle System Dynamics: International Journal of Vehicle Mechanics and Mobility*, Vol. 49, pp.3–28.

Du, Z.X., Wen, X.X. and Shen, Z. (2014) 'The impact analysis of tire parameter for tire wear when monorail vehicle curve driving', *Applied Mechanics and Materials*, Vol. 470, pp.529–533.

Goda, K., Nishigaito, T., Hiraishi, M. and Iwasaki, K. (2000) 'A curving simulation for a monorail car', *Proceedings of the 2000 ASME/IEEE Joint Railroad Conference, 2000*, ASME/IEEE Joint, Newark NJ, pp.171–177.

Liu, G. *et al.* (2014) 'Effect of wheel pressure on vibration of straddle monorail transit vehicle-bridge system', *Advanced Materials Research*, Vol. 919, pp.542–546.

Mohajer, N., Abdi, H., Nelson, K. and Nahavandi, S. (2015) 'Vehicle motion simulators, a key step towards road vehicle dynamics improvement', *Vehicle System Dynamics*, Vol. 53, pp.1204–1226.

Pacejka, H.B. (2005) *Tire and Vehicle Dynamics*, Elsevier.

Polach, O. (2007) 'Comparability of the non-linear and linearized stability assessment during railway vehicle design', *Vehicle System Dynamics: International Journal of Vehicle Mechanics and Mobility*, Vol. 44, No. Supp. 1, pp.129–138.

Segel, L. and Ervin, R.D. (1981) 'The influence of tire factors on the stability of trucks and tracktor trailers', *Vehicle System Dynamics*, Vol. 10, No. 1, pp.39–59.

Shabana, A.A. (2008) *Railroad Vehicle Dynamics: A Computational Approach*, CRC Press.

Shen, S., Wang, J., Shi, P. and Premier, G. (2007) 'Nonlinear dynamics and stability analysis of vehicle plane motions', *Vehicle System Dynamics: International Journal of Vehicle Mechanics and Mobility*, Vol. 45, pp.15–35.

Wei, T. and Dorfi, H.R. (2014) 'Tire transient lateral force generation: characterization and contribution to vehicle handling performance', *Tire Science And Technology*, Vol. 42, No. 4, pp.263–289.